Numerical Study on Variation of Feedback Methods in Ultrasonic-Measurement-Integrated Simulation of Blood Flow in the Aneurysmal Aorta*

Kenichi FUNAMOTO**, Toshiyuki HAYASE***, Yoshifumi SAIJO**** and Tomoyuki YAMBE****

The complicated relationships between hemodynamics and aneurysms have been investigated intensively. However, existing methodologies have inherent limitations in providing real blood flow fields. The authors have proposed Ultrasonic-Measurement-Integrated (UMI) simulation, in which the feedback signals lead to convergence of the calculated blood flow structure to the real one even with incorrect boundary/initial conditions. In UMI simulation, determination of the feedback law is substantially important, but detailed particulars remain to be accounted for. In this paper, first, the effects of density of feedback points and feedback domains are systematically investigated. Improvement of computational accuracy in the feedback domain is achieved even in low density of feedback points of 25%, and such improvement persists in the downstream region. Secondly, the most effective combination of feedback gains for momentum and pressure equations is investigated, confirming the validity of the simple condition to use the same value for the velocity and pressure gains.

Key Words: Bio-Fluid Mechanics, Computational Fluid Dynamics, Flow Visualization, Pulsation, Measurement-Integrated Simulation, Ultrasonic Measurement, Feedback Law, Blood Flow, Aneurysm

1. Introduction

Aortic aneurysm is a circulatory disease, which is caused by degeneration of a blood vessel, resulting in its extending like a balloon. The complicated relationships between hemodynamics and aneurysms have been elucidated by experimental measurement and numerical simulation. From the macro point of view, hemodynamic stresses such as wall shear stress and pressure distribution on the blood vessel wall in an aneurysm play important roles in the development, progress and rupture of aneurysms[(1)-(4)]. At the cell level, it is reported that the endothelial cells of the blood vessel respond to low wall shear stress and large spatial gradients[(5),(6)]. However, there is presently no criterion indicative of the advisability of surgery except for empirical indications such as the size or the aspect ratio[(7),(8)].

For the development of more accurate diagnosis or treatment of aneurysms, a method to obtain detailed hemodynamic data regarding the aneurysm is essential. With existing medical imaging techniques such as MRI, CT and ultrasonography, it is difficult to obtain detailed information of the blood flow structure due to the limitations of each method. To obtain comprehensive information, many studies have been conducted with a combination of measurement and numerical simulation; for example, blood flow simulation has been carried out using realistic vessel geometries obtained by measurement[(9),(10)]. However, such research did not pay much attention to the problem of specification of the boundary conditions. Boundary conditions are a substantive and indispensable issue for numerical simulation since they usually affect the computational results, especially for the blood flow in a complicated geometry[(11),(12)]. Nowadays, owing to the improvement of MR angiography, the velocity profile on the cross-section of a blood vessel can be obtained. Some papers have dealt with the numerical simulation in which realistic ve-

* Received 9th June, 2005 (No. 05-4071)
** Graduate School of Engineering, Tohoku University, 6–6–01 Aramaki-Aoba, Aoba-ku, Sendai 980–8579, Japan
*** Institute of Fluid Science, Tohoku University, 2–1–1 Katahira, Aoba-ku, Sendai 980–8577, Japan. E-mail: hayase@ifs.tohoku.ac.jp
**** Institute of Development, Aging and Cancer, Tohoku University, 4–1 Seiryo-cho, Aoba-ku, Sendai 980–8575, Japan

locity profiles are applied at the upstream boundary and in which realistic vessel geometries are employed[12),(13)]. Marshall et al.[13)] carried out a computational fluid dynamics study in a healthy and stenosed rigid model of the carotid bifurcation with realistic boundary conditions based on MR measurement data and revealed that differences existed between the results obtained by computation and those forthcoming from measurement. Their study also demonstrated the efficacy of numerical simulation[13)]. However, since the precision of MR measurement is still not so high[12)–14)], error may be introduced to the numerical simulation, and thus calculated hemodynamics inevitably includes error. Hence, a method to reduce the error of the calculated flow is required in order to realize advanced accurate diagnosis and treatment.

For this purpose, we have proposed Ultrasonic-Measurement-Integrated (UMI) simulation[15)], introducing the concept of flow observer to blood flow simulation to reproduce the real blood flow numerically with the aid of feedback from measurement[16)–18)]. In other fields, Hayase et al. applied flow observer to a turbulent flow through a square duct[16)], and Nisugi et al. developed a hybrid wind tunnel and investigated the flow with a Karman vortex street[17),18)]. Note that, the UMI simulation treated in this paper is different from the authors' other work on turbulent flow or Karman vortex street mentioned above in the respect that the present work assumes incorrect boundary condition. A block diagram of UMI simulation is shown in Fig. 1. This methodology integrates ultrasonic measurement and numerical simulation by feedback which is determined from the difference between the two methods and applied to the simulation. Ultrasonic measurement is the most widely available since the equipment used is relatively inexpensive and compact. Color Doppler imaging[19)] enables us to display real-time images of the vessel configuration by reconstructing time delays and magnitudes of the echo of the ultrasonic beam. The velocity component in the ultrasonic beam direction (Doppler velocity) can also be obtained by measuring the Doppler shift frequency. However, realistic three-dimensional blood flow structure and pressure distribution cannot be directly obtained by ultrasonic measurement. Though many investigations have been carried out[20)–22)], there are various limitations such as the direct effects of noise and the sensitivity of the positioning of the Doppler transducer on data acquisition or the assumption of symmetrical flow in the calculation. No existing system provides complete information on blood flow in real time. In UMI simulation, numerical simulation is first carried out with assumed boundary conditions. At selected grid points, defined as feedback points, the discrepancy between the measured Doppler velocity and the one estimated by numerical simulation is evaluated, and then feedback signals are generated from it based on the feedback law. These signals are fed back to the governing equations of the numerical simulation as a source term in order to compensate for the difference and to realize convergence of the computational result to the real flow.

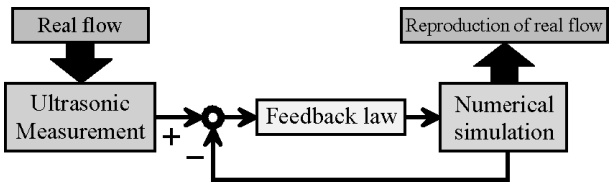

Fig. 1 Schematic diagram of UMI simulation

The feedback law is crucially important in UMI simulation, but its design depends on the performer and is determined through trial and error. Detailed particulars remain to be accounted for. In a former study[15)], the authors numerically investigated the efficiency of UMI simulation using a two-dimensional model problem of blood flow in an aneurysmal aorta. The work defined two rectangular feedback domains, which covered an aneurysm or the blood vessel around the aneurysm, and applied feedback at all grid points in those domains. Two formulae were also introduced as feedback formulae in the UMI simulation: In one formula (feedback A), feedback was applied only to the momentum equation, while in the other formula (feedback B), an additional feedback signal was also applied to the pressure equation.

The present paper deals with further investigation of the feedback law of UMI simulation using the same two-dimensional model problem as that of the former study[15)]. First, the effects of the arrangement of feedback points are investigated. The density of feedback points is changed in the two rectangular feedback domains. The location of the feedback domain is also changed to investigate how the feedback influences the upstream or downstream region of the feedback domain and the location of the most effective position of the feedback domain for reproduction of the blood flow in the aneurysm. Secondly, for feedback formula B, the effect of feedback gains (K_v,K_p) on momentum and pressure equations is investigated. In the former study[15)], for the sake of simplicity, limited conditions $K_v = K_p$ were investigated. In the present study, however, the optimum combination of the multiple feedback gains is investigated by changing them in two-dimensional parameter space.

2. Subject and Method for UMI Simulation

2.1 Subject and measurement method

This paper deals with two-dimensional model blood flow around a thoracic aneurysm. The subject (a 62-year-old male patient with a chronic aortic aneurysm in his descending aorta), as well as the measurement devices and method [an ultrasound device (SONOS 5500, Philips Medical Systems, Andover, MA, USA) with a trans-

esophageal ultrasonic transducer (T6210, Philips Medical Systems, Andover, MA, USA)] in this study were the same as those in the former work[15]. Ultrasonic measurement was carried out with a color Doppler imaging technique from inside the esophagus. Note that color Doppler ultrasonography measured the velocity component in the ultrasonic beam direction as well as the blood vessel configuration of descending aorta with a chronic aneurysm[19]. In this study, we used the measured vessel configuration, not the measured Doppler velocity, since the latter did not provide data on the velocity vector or pressure which were necessary to evaluate the accuracy of UMI simulation. Alternatively, we defined a standard solution of the numerical simulation with a supposed boundary condition as a model of the real blood flow and used the Doppler velocity calculated from the standard solution for feedback in UMI simulation. We performed UMI simulation and ordinary simulation using the same geometry as the standard solution but different boundary condition. UMI simulation using real color Doppler measurement was presented in the earlier report[15].

2.2 Numerical simulation

Though intravascular blood flow in vivo has a complex three-dimensional structure, we assumed a two-dimensional flow for the fundamental study of UMI simulation. Governing equations for a two-dimensional incompressible and viscous fluid flow are the Navier-Stokes equations,

$$\rho\left(\frac{\partial \mathbf{u}}{\partial t}+(\mathbf{u}\cdot\mathrm{grad})\mathbf{u}\right)=-\mathrm{grad}\,p+\mu\nabla^2\mathbf{u}, \tag{1}$$

and the equation of continuity,

$$\mathrm{div}\mathbf{u}=0, \tag{2}$$

where $\mathbf{u}=(u,v)$ is the velocity vector, p is the pressure. The governing equations were discretized by means of the finite volume method and solved with an algorithm similar to the SIMPLER method[15),(23),(24)]. In the SIMPLER method, the x-directional momentum equation is expressed as

$$u_i=\left(\sum B_j u_j+S_i\right)/B_i+d_i(p_i-p_{i-1}), \tag{3}$$

where (Σ B_j u_j) means the summation of the four values circumfusing u_i. By substituting Eq. (3) and similar equations for y-directional momentum in the integrated form of the equation of continuity, the pressure equation is obtained as

$$a_i p_i=\sum a_j p_j+s_{pi}, \tag{4}$$

where (Σ a_j p_j) means the summation of the values at four adjacent nodes. The notations of the parameters in Eqs. (3) and (4), as well as supplementary pressure correction equations and velocity correction procedure in SIMPLER method were explained in the Ref. (24). Feedback signals added to Eqs. (3) and (4) in the governing equations of UMI simulation will be explained later.

Table 1 shows the parameters used in this computation. Cardiac cycle T was calculated from the heart rate. The upstream shape of the blood vessel was assumed to be cylindrical, and the diameter D was calculated from the image. Since the upstream boundary was located at some distance from the aneurysm, we considered that the blood vessel could be assumed to be cylindrical. Referring to the blood flow measurement data[25], we assumed that 30% of the cardiac output flowed into the branches and the remaining 70% (6.42×10^{-5} $\mathrm{m^3s^{-1}}$) flowed into the descending aorta. The variation of the flow rate q was modeled as shown in Fig. 2 according to the MR measurement by Olufsen et al.[26] The maximum average flow velocity at the upstream boundary $u'_{\max}$ was determined by dividing the maximum flow rate by the circular cross-sectional area of the inlet (see Table 1). Blood was assumed to be Newtonian fluid with a density $\rho=1.0\times10^3$ $\mathrm{kgm^{-3}}$ and a dynamic viscosity $\mu=4.0\times10^{-3}$ Pas within normal range. All the values were nondimensionalized with the entrance vessel diameter D, the maximum average flow velocity at the upstream boundary $u'_{\max}$, and the kinematic viscosity ν of the blood. Note that we used $u'_{\max}$ in normalizing the feedback signal or error norms. From here on, the same symbols are used for both dimensional and nondimensional values since it does not cause confusion.

The B-mode image of the blood vessel obtained by ul-

Table 1 Computational conditions

Heart rate	0.87 Hz
Cardiac cycle T	1.15 s
Cardiac output	9.17×10^{-5} $\mathrm{m^3/s}$
Entrance flow	6.42×10^{-5} $\mathrm{m^3/s}$
Maximum average velocity $u'_{\max}$	0.74 m/s
Entrance vessel diameter D	2.83×10^{-2} m
Kinematic viscosity ν	4.0×10^{-6} $\mathrm{m^2/s}$
Computational time step Δt	0.01 s

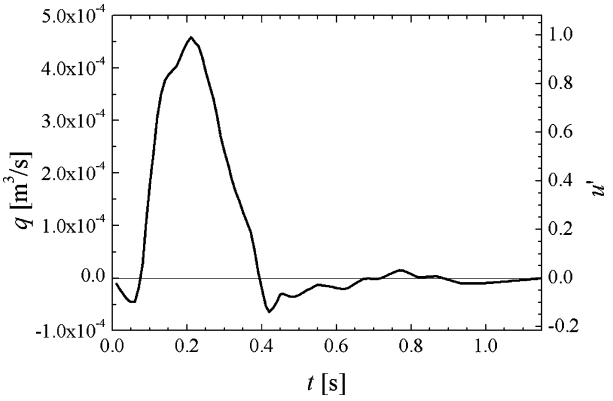

Fig. 2 Time-variation of flow rate (dimensional) and cross-sectional average flow velocity at upstream boundary (nondimensional)

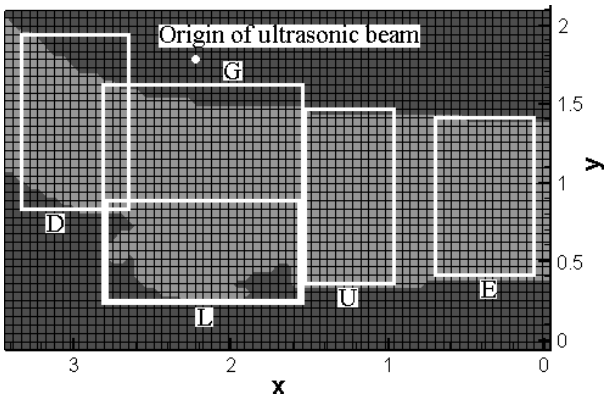

Fig. 3 Computational domain and feedback domains (nondimensional)

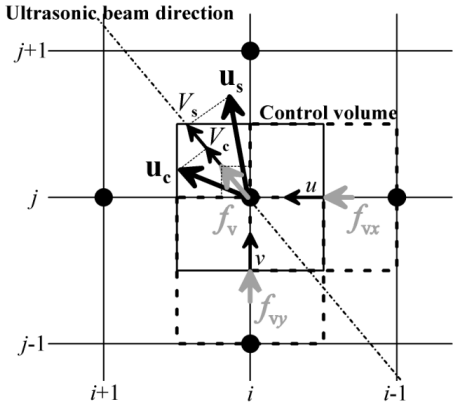

Fig. 4 Calculation of feedback signal on staggered grid system

trasonic diagnostic equipment was digitized to extract the cross-sectional surface manually, and the pixel data was allocated to define a two-dimensional computational domain as shown in Fig. 3. The shape of the blood vessel in the figure was extended from the ultrasonic image around 3.5 cm (1.24) in the upstream direction and around 1.5 cm (0.53) in the downstream direction in order to perform numerical simulation (see Fig. 3, the right side is upstream). The x-axis was defined in the flow direction with the origin at the upstream boundary, and the y-axis was defined as shown in Fig. 3. We introduced a staggered grid system with 65×40 grid points in x and y directions with uniform grid spacing of 1.487×10^{-3} m as a compromise between reproducibility of the blood vessel shape and computational time.

With regard to the upstream boundary condition, we assumed a Poiseuille flow, a parallel flow with a parabolic profile in x-directional velocity for the standard solution or the model of real flow. On the other hand, we assumed a different upstream boundary condition with a uniform parallel velocity profile in x-direction for the UMI simulation and the ordinary simulation since we do not usually know the correct boundary condition of the real flow. The error was introduced in the UMI and ordinary simulations against the standard solution. After test computations, the maximum iteration number and the tolerance of residual for convergence were determined as 300 and 1×10^{-5}, respectively.

2.3 Feedback algorithms

In UMI simulation in this paper, we dealt with two feedback formulae proposed in the former study[15]: the feedback to the velocity field (feedback A) and the feedback to the velocity and pressure fields (feedback B). Feedback A applies the artificial force f_v proportional to the difference between Doppler velocity V of the standard solution (model of the real flow) and that of the UMI simulation to the Navier-Stokes equations in the direction of the ultrasonic beam (see Fig. 4). The artificial force f_v is calculated by the following equation:

$$f_v = -K_v \rho (V_c - V_s)\, u'_{max} \Delta S, \tag{5}$$

where K_v is the feedback gain (nondimensional), V_c and V_s are the Doppler velocities of UMI simulation and standard solution, which are projections of velocity vectors $\mathbf{u}_c$ and $\mathbf{u}_s$ in the ultrasonic beam direction as shown in Fig. 4, respectively, u'_{max} is the maximum average flow velocity of the blood at the upstream boundary, and ΔS is an interfacial area of the control volume of pressure. For instance, in the case that V_c is smaller than V_s as shown in Fig. 4, f_v accelerates the fluid to reduce the discrepancy in the ultrasonic beam direction in UMI simulation. In the actual computational operation, f_v is decomposed to the x-directional and y-directional components, f_{vx} and f_{vy}, which are added to the control volume of $u(i, j)$ and $v(i, j)$ in each directional Navier-Stokes equation, respectively.

In feedback B, an additional feedback signal s_p is introduced to the pressure equation as the source term to counteract the effect of the artificial force f_v in the momentum equations. The signal s_p is calculated by the following equation:

$$s_p = -K_p \rho (V_c - V_s) \Delta S, \tag{6}$$

where K_p is the feedback gain for the pressure (nondimensional). In Fig. 4, if the pressure in the control volume of pressure $p(i, j)$ increases by the addition of the feedback signal f_v in Eq. (5), the source term s_p in the pressure equation acts to reduce the increased pressure. Further discussion on the calculation of the feedback signals is given in the previous article[15].

UMI simulation is specified by the feedback gain K_v for feedback A or by the combination of feedback gains K_v and K_p for feedback B. Note that the special case of feedback B with $K_p = 0$ means feedback A, and that with $K_v = K_p = 0$ means the ordinary simulation without feedback.

We defined several sub-domains in which feedback points were arranged in a flow domain as shown in Fig. 3. In order to evaluate the effect of density of feedback points on the computational accuracy of the blood flow fields in the aneurysm, two feedback domains, G and L, which

Table 2 Arrangements of feedback points, and optimum and critical gains for feedback A and B

	Feedback point		Optimum gain (left) and Critical gain			
	Number	Density	Feedback A		Feedback B	
G1	546	1.000	0.4	0.5	0.2	0.3
G2	140	0.256	0.8	0.9	0.8	0.9
G4	37	0.068	1.1	1.2	1	1.1
G8	10	0.018	1.1	1.3	1	1.3
L1	253	1.000	0.4	0.5	0.3	0.4
L2	68	0.269	0.8	0.9	0.6	0.9
L3	31	0.123	1	1.1	1	1.1
L4	21	0.083	1.1	1.2	1.1	1.2
L6	10	0.040	0.9	1.3	1.2	1.3
L8	5	0.020	1.1	1.2	0.6	1.2

were the same as those in the previous study[15], were defined. The domain L locally covered the aneurysmal region, while the domain G globally covered the aneurysm including the main branch to investigate the effect of the feedback on the computational accuracy of blood flow field in main branch. In the two domains, density of the feedback points was changed. The regions of global and local feedback domains contained 675 and 325 grid points, respectively. We defined the arrangement G1 as that in which all the grid points in the fluid region of the global domain G were assigned as feedback points. Consequently, 546 out of 675 grid points were defined as feedback points in the G1 arrangement. In addition, arrangements G2, G4 and G8 were defined so that feedback points were located at every 2, 4, or 8 grid points in each coordinate direction starting from the grid point at upper left corner of domain G, respectively. The same procedure was done for the local domain L, and arrangements termed L1, L2, L3, L4, L6 and L8 were defined. Here, the density of feedback points was calculated by dividing the number of feedback points by the number of the grid points in the fluid region in each feedback domain. Detailed information on each arrangement is described in Table 2.

The other feedback domains, domain E, U and D, which included almost the same number of grid points in the fluid region as that of domain L, were defined in order to verify the effects of the feedback in the upstream and downstream regions of the feedback domains, and also to investigate the effective position of the feedback domain for reproduction of the blood flow in the aneurysm. For purposes of comparison, we investigated using the E1, U1, L1 and D1 arrangements consisting of all the fluid points in the domains. The exact number of feedback points in each feedback arrangement is described in Table 3.

As the Doppler velocity V is the velocity component in the beam direction, the position of the origin of the ultrasonic beam affects the Doppler velocities at the feedback points and, therefore, the result of UMI simulation. In this study, the origin of the ultrasonic beam was set at the probe position in the ultrasonic measurement as shown in Fig. 3, which was the same position as that in the previous study[15].

Table 3 Arrangements of feedback points, optimum and critical gains, and average error norms in local domain L

Feedback	Domain	Number of feedback points	Optimum gain	Critical gain	$\bar{e}_{\mathrm{L}}^{*}(\mathbf{u})$	$\bar{e}_{\mathrm{L}}^{*}(p)$
A	E1	251	0.4	0.5	0.771	0.625
	U1	253	0.2	0.6	0.879	0.913
	L1	253	0.4	0.5	0.433	0.853
	D1	253	0.2	0.5	0.926	0.798
B	E1	251	0.1	0.3	0.465	0.360
	U1	253	0.2	0.3	0.319	0.305
	L1	253	0.3	0.4	0.432	0.607
	D1	253	0.1	0.3	0.655	0.559

2.4 Error evaluation

For the evaluation of UMI simulation, the error norm $e_n(a)$ was defined at the grid point n for an arbitrary variable a, which may be the velocity vector $\mathbf{u}$, the velocity component u, v, or V, or pressure p, by the following equation:

$$e_n(a) = \frac{1}{a_{\max} T} \int_T |a_{cn}(t) - a_{sn}(t)|\, dt, \tag{7}$$

where T is the cardiac cycle, $|\bullet|$ is the absolute value for scalar variables or the l_1 norm $|u|+|v|$ for the velocity vector $\mathbf{u}$, $a_{\max}$ is the characteristic value for normalization: $a_{\max} = u'_{\max}$ for velocity or $a_{\max} = \rho u'^{2}_{\max}$ for pressure. Subscript cn corresponds to the computation, i.e., UMI simulation or ordinary simulation, at the grid point with index n, and sn corresponds to the standard solution at the same grid point. In addition, the average error norm $\bar{e}_{\Omega}(a)$ was defined over the monitoring points in a domain Ω by the following equation:

$$\bar{e}_{\Omega}(a) = \frac{1}{N} \sum_{\mathbf{x}_n \in \Omega} e_n(a). \tag{8}$$

The domain Ω is arbitrarily chosen for the purpose of evaluation. For example, all 675 or 325 grid points in the global feedback domain G or local feedback domain L were used for $\bar{e}_{\mathrm{G}}(a)$ or $\bar{e}_{\mathrm{L}}(a)$; grid points on each transverse cross-section of the flow domain were used to calculate the cross-sectional average error norm, $\bar{e}_{\mathrm{C}(x)}(a)$. In order to clearly demonstrate the reduction of error in UMI simulation from that of the ordinary simulation, we introduced normalized average error norm $\bar{e}_{\Omega}^{*}(a)$ as the average error norm of the UMI simulation divided by that of the ordinary simulation.

The optimum gain for each feedback algorithm was defined as the gain or the set of gains that minimized the average error norm $\bar{e}_{\Omega}(a)$ for the arbitrary variable a in the feedback domain Ω by extending the definition of the previous research[15].

3. Results and Discussion

All computations were performed using the supercomputer system SGI ORIGIN 2000 in the Advanced Fluid Information Research Center, Institute of Fluid Science, Tohoku University. Investigation of the effect of the

density of feedback points in UMI simulations on computational accuracy in the domain was first carried out using two feedback domains and two feedback formulae. The error norms were used for the evaluation. The effect of the location of feedback domain was then investigated using four different arrangements of feedback points by calculating the cross-sectional average error norm at each transverse cross-section of the blood vessel. Lastly, the assumption for feedback B of $K_v = K_p$ was removed and UMI simulation was performed by changing those two feedback gains independently, searching the optimum gains for the various average error norms. All computations were performed for a number of cardiac cycles until the periodical solution was obtained.

3.1 Density of feedback points

For evaluation of the effect of the density of feedback points in the feedback point arrangements G and L (see Fig. 3), the optimum and critical gains were first obtained for each feedback point arrangement and feedback formula. For UMI simulation with feedback A, K_p was fixed at zero and K_v was increased from zero by increments of 0.1 until the computation diverged for each arrangement of feedback points. Generally, as K_v increases, the average error norms of velocity components decrease and converge to each constant value, though that of pressure slightly increases. For feedback B, we searched in a limited condition of $K_v = K_p$ here[15], changing K_v and K_p by 0.1 for each arrangement for the sake of simplicity. Study of the full (K_v, K_p) parameter plane is discussed in a later section. In this section, we defined the optimum gain at which the average error norm $\bar{e}_\Omega(\mathbf{u})$ of velocity vector $\mathbf{u}$ in each feedback domain became minimum, and the critical gain at which the computation diverged. Table 2 summarizes the results for the cases investigated.

Figure 5 shows the streamlines at $t = 0.35$ s in the deceleration phase for the standard solution, the ordinary simulation and the UMI simulation, respectively. In the standard solution [Fig. 5 (a)], recirculation regions exist in the blood vessel, and one large vortex is observed in the aneurysm in this phase. Because of the different upstream boundary condition, the streamlines of the ordinary simulation in Fig. 5 (b) are different from those of the standard solution in Fig. 5 (a), especially in the aneurysm. Figure 5 (c) shows the streamlines obtained by UMI simulation with the optimum gain for feedback B using the G1 arrangement (see Table 2). Although the streamlines near the upstream boundary are very similar to those of the ordinary simulation because of the same incorrect upstream boundary condition, they become similar to those of the standard solution in the feedback domain due to the effect of the feedback.

Figure 6 compares the distributions of the error norms for u, v, V and p in the global domain G between UMI simulations with feedback B using the G1, G2, G4, or G8 arrangement of feedback points and the ordinary simulation without feedback. In the ordinary simulation, a large error shown by bright color arises in the domain G. On the other hand, in the UMI simulation with the G1 arrangement, the error is almost eliminated and the white region disappears for all variables. Comparing the results of UMI simulations with different arrangements, the greater the number of feedback points, the better the computational accuracy. As the interval between feedback points increases, relatively large error occurs at the grid points which are not the feedback points. However, even in UMI simulation with the G8 arrangement using only 10 feedback points (see Table 2), which is about 1/55 of G1 arrangement, improvement is still achieved in comparison with the ordinary simulation.

The average error norms, $\bar{e}_G$ and $\bar{e}_L$, in the global and

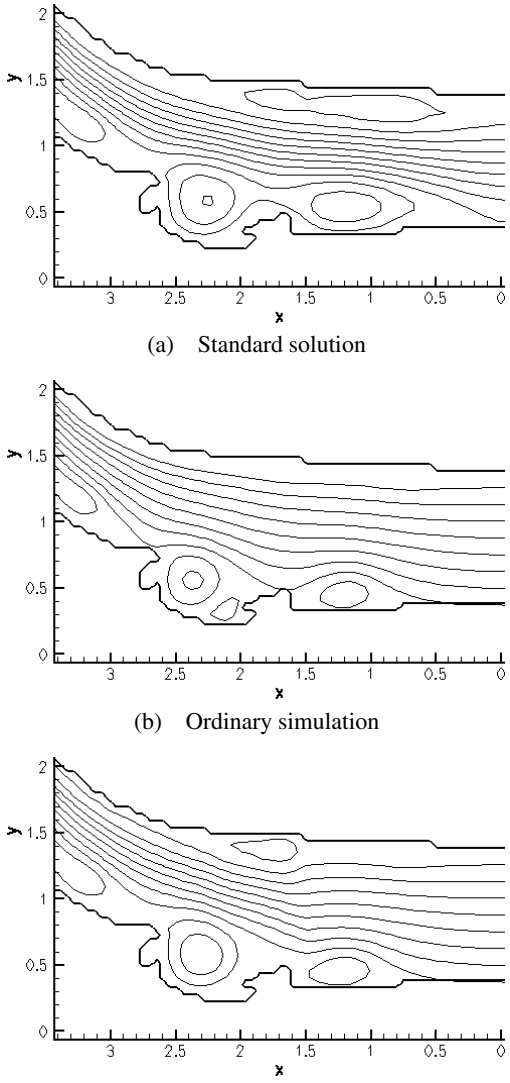

(a) Standard solution

(b) Ordinary simulation

(c) UMI simulation, G1 arrangement, $(K_v, K_p) = (0.2, 0.2)$

Fig. 5 Comparison of streamlines at $t = 0.35$ s in deceleration phase between the standard solution, the ordinary simulation and UMI simulation (nondimensional)

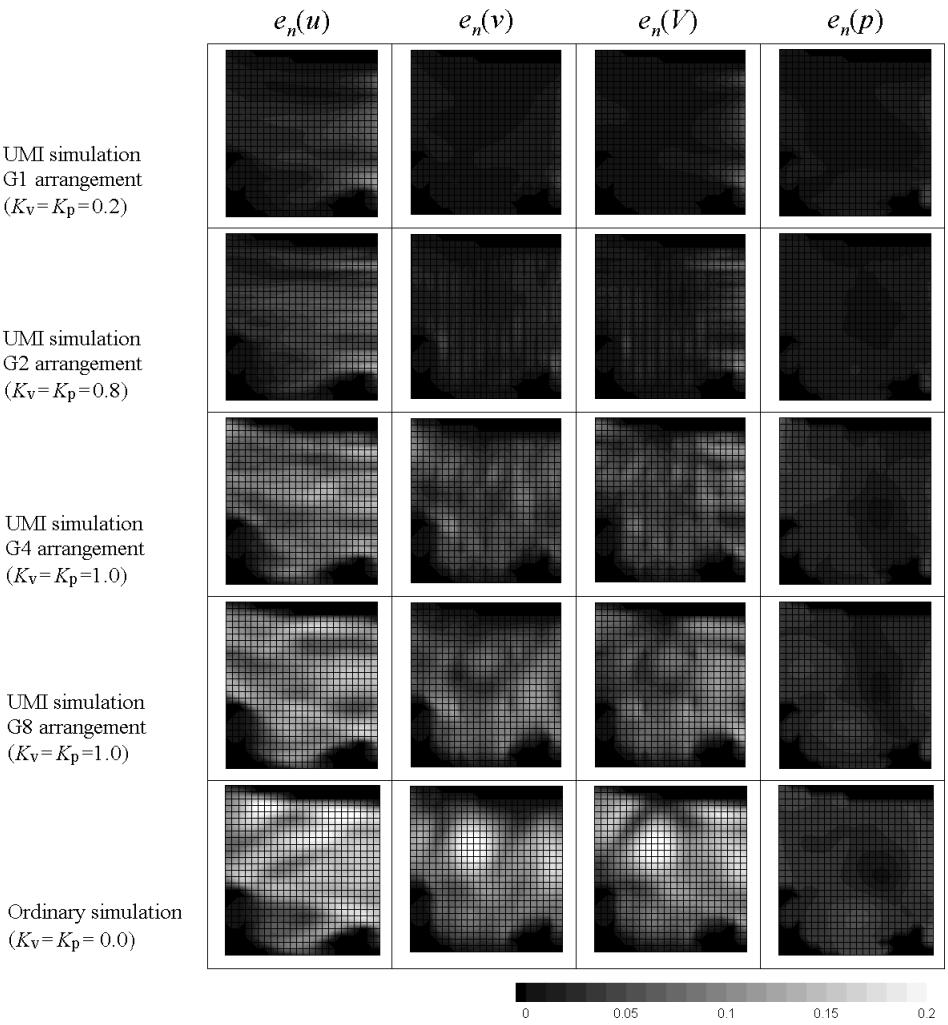

Fig. 6 Distributions of error norm of each variable of UMI simulations with feedback B and the ordinary simulation

local feedback domains were calculated for the UMI simulations with global arrangements (G1, G2, G4 and G8) and local arrangements (L1, L2, L3, L4, L6 and L8) to investigate the change of improvement of the computational accuracy resulting from the decrement of feedback points. Figure 7 (a) and (b) show the average error norms of the velocity vector **u** in domains G and L with the number of feedback points, respectively. The computational accuracy of each UMI simulation depends on the arrangement of feedback points as well as the domain where the error norm is evaluated. It is noted that feedback A and B with global arrangement G result in almost the same precision in velocity field for more than 100 feedback points. Comparing the average error norms with the L1 and G1 arrangements, indicated by dotted and solid circles, the results are close for $\bar{e}_L(\mathbf{u})$ in Fig. 7 (b) but not for $\bar{e}_G(\mathbf{u})$ in Fig. 7 (a); showing that the local arrangement provides more improvement in the local feedback domain than in the global feedback domain. The G2 arrangement provides more reduction of $\bar{e}_L(\mathbf{u})$ as well as $\bar{e}_G(\mathbf{u})$ than the L1 arrangement. In this study, the large error against the standard solution mainly occurred in the large branch above the aneurysm as observed in Fig. 6, and it may deteriorate the computational accuracy in the aneurysm of UMI simulation. Therefore, when the number of feedback points is fixed, it is better to arrange feedback points covering the region where large error exists even if the density of feedback points decreases to some extent.

The results mentioned above were rearranged as a function of the density of feedback points. Figure 8 shows the average error norm normalized with that of the ordinary simulation in the feedback domain G or L with the density of feedback points. In Fig. 8, the two lines of each feedback points arrangement exist in close proximity, showing sharp decrease of error norm of velocity vector as the density of feedback points increases in the range of relatively low density. This implies that the error does not increase much when the density of feedback points is reduced from 1. The effect of anisotropic arrangement of feedback points remains as a future work.

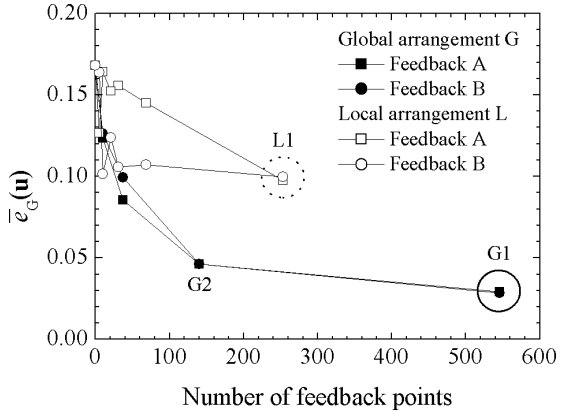

(a) Error norm in global feedback domain

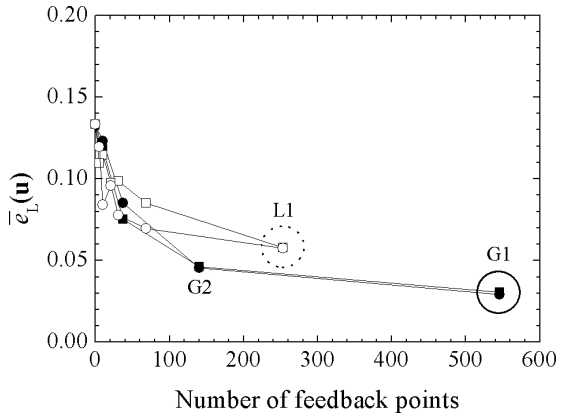

(b) Error norm in local feedback domain

Fig. 7 Average error norm of velocity vector of UMI simulation as a function of number of feedback points

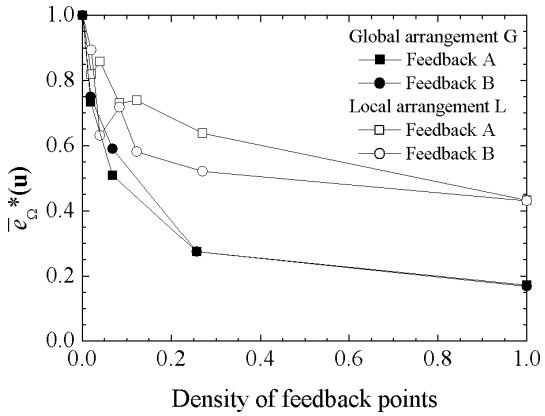

Fig. 8 Normalized average error norm of velocity vector in the feedback domain as a function of density of feedback points

The computational time for one cardiac cycle and the cycles necessary to obtain periodic oscillations are shown in Fig. 9. Concerning the computational time for 1 cardiac cycle in Fig. 9 (a), UMI simulations with feedback A take slightly longer time than the ordinary simulation shown by a dotted line, while UMI simulations with feedback B require computational time about 1.5 times longer.

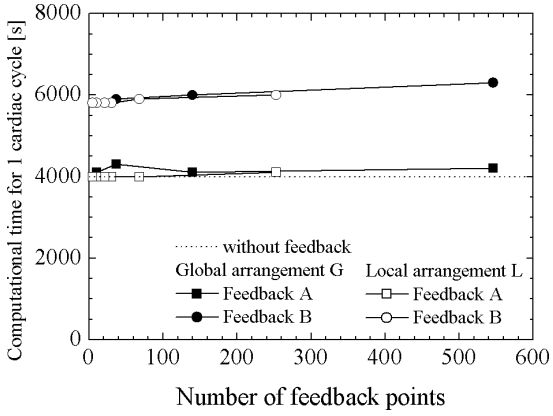

(a) Computational time for 1 cardiac cycle

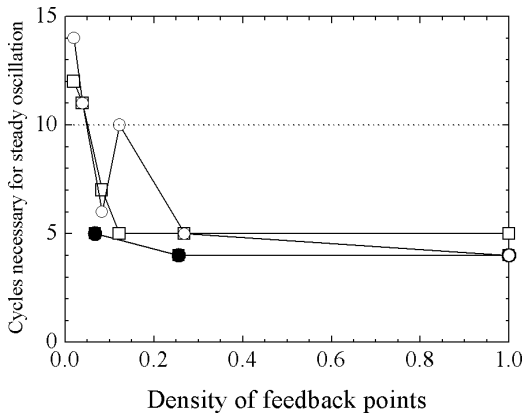

(b) Cardiac cycles necessary to reach steady oscillation

Fig. 9 Relationship between the computational load to obtain final solution and feedback points

Variation of the computational time with number or arrangement of the feedback points is small. In contrast, the number of cardiac cycles necessary to obtain steady oscillation in Fig. 9 (b) substantially decreases with the density of feedback points in UMI simulations. Eventually, the UMI simulation requires more computational time for a fixed time interval, but overall computational time needed to obtain a final solution is less than that of the ordinary simulation if the density of feedback points is sufficiently large.

3.2 Location of feedback domain

In the preceding section, we considered the number of feedback points using two feedback domains, G and L, near the aneurysm. In this section, we considered the location of the feedback domain using four arrangements (E1, U1, L1 and D1) of almost the same number of feedback points in different locations in the flow domain (see Fig. 3 and Table 3).

In this section, optimum and critical gains were determined with respect to the average error norm $\bar{e}_L(\mathbf{u})$ of velocity vector $\mathbf{u}$ in local feedback domain L in order to reproduce the blood flow field in the aneurysm. The results are summarized in Table 3. For all arrangements,

feedback B gives better results than feedback A for both the velocity vector and the pressure. The computational accuracy depends on the location of the feedback domain. UMI simulation with feedback B using the U1 arrangement yields the best result for reproduction of the blood flow field in the aneurysm; $\bar{e}_{\mathrm{L}}(\mathbf{u})$ and $\bar{e}_{\mathrm{L}}(p)$ are reduced to 32% and 31%, respectively. UMI simulations with E and U which are located upstream from the domain L result in the relatively good improvement than that of UMI simulation using feedback domain D downstream from the domain L.

The local effect of feedback in the whole computational domain was evaluated for UMI simulations with feedback A with $K_{\mathrm{v}} = 0.2$ and feedback B with $K_{\mathrm{v}} = K_{\mathrm{p}} = 0.1$. For each case, the average error norm was evaluated for velocity vector and pressure over the transverse cross-section as the domain Ω. Figures 10 and 11 show the x-directional variations of the cross-sectional average error norms for velocity vector and pressure of UMI simulation for those cases, respectively. Here, the grey zone enwinding each line shows the region where the feedback is applied. In Fig. 10 (a), improvement of computational accuracy of velocity is achieved due to the application of feedback A, except for the result using the D1 arrangement. The reason for the deterioration of UMI simulation with feedback A using the D1 arrangement of feedback points seems to be the adverse effect on the pressure by the application of feedback signal f_{v}. Figure 10 (b) shows error in pressure extremely increases for domain D. This figure also shows increase of the error of pressure in the feedback domain of the UMI simulation with the E1 arrangement, implying that pressure becomes incorrect in case that the feedback domain is set near the upstream or downstream boundary. On the other hand, feedback B in Fig. 11 can cancel the error in the pressure field to some extent owing to additional feedback to the pressure field as well as the reduction of the error in the velocity field. In Fig. 11 (b), improvement of computational accuracy is observed in the pressure field in UMI simulation with the E1 and D1 arrangements. Moreover, comparing results obtained using domain L with those by the other domains, it can be seen that domains E, U and D, which cover the whole blood vessel, can provide lower minimum values of $\bar{e}_{\mathrm{C}(x)}(\mathbf{u})$. This is because those domains can improve the computational accuracy on the whole cross-section of the blood vessel in the domains.

According to the above discussion on variations of the cross-sectional average error norms, it is confirmed

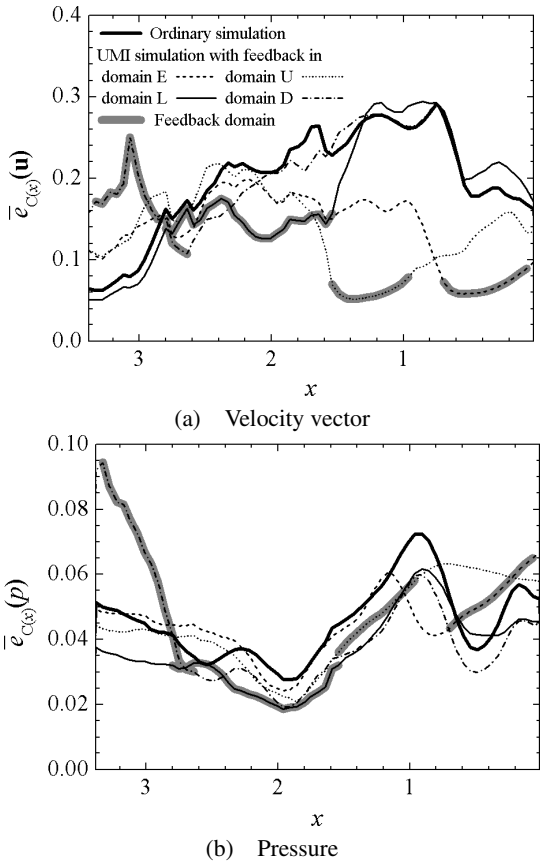

(a) Velocity vector

(b) Pressure

Fig. 10 Average error norms at each cross-section of UMI simulations with feedback formula A ($K_{\mathrm{v}} = 0.2$) and ordinary simulation (nondimensional)

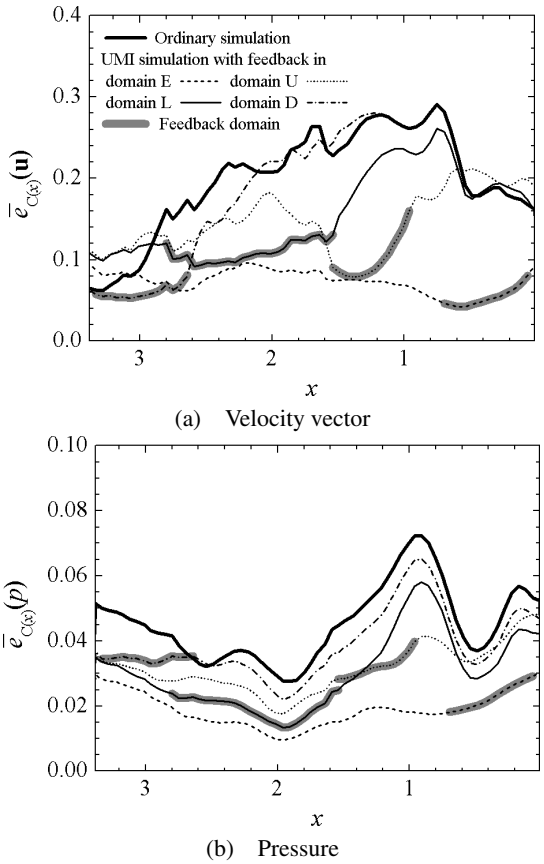

(a) Velocity vector

(b) Pressure

Fig. 11 Average error norms at each cross-section of UMI simulations with feedback formula B ($K_{\mathrm{v}} = K_{\mathrm{p}} = 0.1$) and ordinary simulation (nondimensional)

that the location of the feedback domain plays an important role in UMI simulation. Assignment of the feedback domain to the region upstream of the aneurysm is effective, while assignment of the domain to the region near the upstream or downstream boundary should be avoided, especially for UMI simulation with feedback A. In addition, it is also desirable that the feedback domain cover the whole blood vessel to properly reproduce the blood flow field. Though the arrangement of the feedback domain exactly covering the aneurysmal part has possibility to reproduce the blood flow field locally in the aneurysm, large error surrounding the region may affect the computational accuracy, and, therefore, arrangement of somewhat large feedback domain probably gives a better result.

Comparing two feedback formulae, they have almost the same reproducibility of the velocity field of the standard solution. Feedback B is superior to feedback A for the reproduction of pressure field, but feedback B requires more computational time than feedback A as described above. Hence, it is necessary to choose a proper feedback formula based on the purpose of analysis.

3.3 Optimum feedback gain for feedback B

Although UMI simulation with feedback B has two independent feedback gains, K_v and K_p, computations in former sections were carried out in a limited condition of $K_v = K_p$ for simplicity. In this section, we performed UMI simulation with feedback B using the L1 arrangement without this limitation of the feedback gains. They were changed over the combination of gains where the convergent results were obtained: K_v was varied from 0 to 0.4, and K_p was 0 to 0.3 at intervals of 0.1. The results were evaluated by the normalized average error norms, $\bar{e}_L{}^*(\mathbf{u})$, $\bar{e}_L{}^*(p)$ and $[\bar{e}_L(\mathbf{u}) + \bar{e}_L(p)]^*$ in the feedback domain L.

Figure 12 shows the distributions of the normalized average error norms of velocity vector, pressure, and their sum as a function of two feedback gains. Here, each range of the feedback gains in Fig. 12 is where convergent results can be obtained. Based on the normalized average error norm of velocity vector $\bar{e}_L{}^*(\mathbf{u})$, which is used in the former section, the optimum combination of gains is $(K_v, K_p) = (0.4, 0.3)$ with an error norm of 0.057 [circle in Fig. 12 (a)]. In the limited condition that $K_v = K_p$ in the former sections, the optimum feedback gains are determined as $(K_v, K_p) = (0.3, 0.3)$ with an error norm of 0.058 [square in Fig. 12 (a)]. The difference between the errors in these cases is very small. Of course, the different evaluations of the error norms result in different combinations of optimum gains. For example, for the normalized average error norm of pressure $\bar{e}_L{}^*(p)$, the optimum gains become $(K_v, K_p) = (0.1, 0.1)$ with the error norm of 0.014 [circle in Fig. 12 (b)]. For the sum of the average error norms of the velocity and the pressure $[\bar{e}_L(\mathbf{u}) + \bar{e}_L(p)]^*$, optimum feedback gains are $(K_v, K_p) = (0.3, 0.3)$ with the error norm of 0.075 [circle in Fig. 12 (c)].

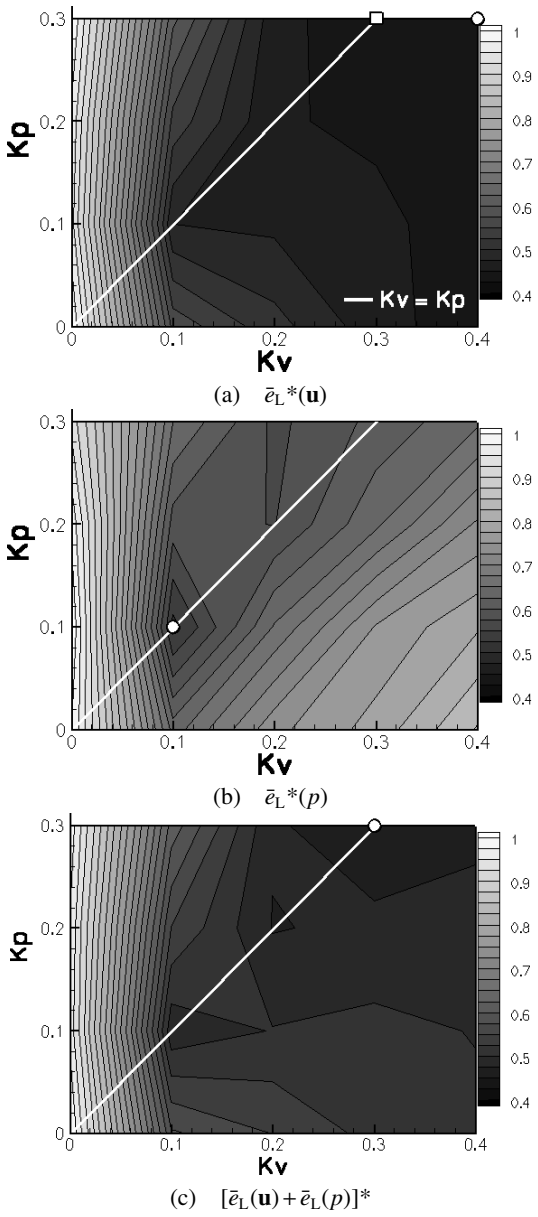

(a) $\bar{e}_L{}^*(\mathbf{u})$

(b) $\bar{e}_L{}^*(p)$

(c) $[\bar{e}_L(\mathbf{u}) + \bar{e}_L(p)]^*$

Fig. 12 Contours of normalized average error norms of different parameters in a two-dimensional parameter space of feedback gains (K_v, K_p) of feedback B with L1 arrangement

According to these results, it is confirmed that the optimization of feedback gains in the limited condition that $K_v = K_p$ provides an approximately optimum result for the velocity, and exactly the optimum results for pressure and the sum of these two. It means that the present result obtained with the limitation of $K_v = K_p$ in feedback B is almost valid in general condition without the limitation. The limitation simplifies the searching of the optimum combination of feedback gains, probably introducing little significant error.

4. Conclusion

This paper has dealt with determination of the feedback in the Ultrasonic-Measurement-Integrated (UMI) simulation in order to reproduce the blood flow field in an aneurysm. A two-dimensional model problem for the descending aorta with an aneurysm was investigated numerically for two feedback formulae A and B: the former applied feedback to the momentum equation and the latter to the momentum and pressure equations; for feedback domains with different density of feedback points; for five different feedback domains; and for different norms to evaluate the error. It was revealed that UMI simulation has a potential to reproduce accurate and detailed blood flow fields in complicated blood geometries even if only limited information of blood flow is obtained by measurement. Results obtained in this study are summarized as follows.

Effects of the density of feedback points were investigated for two feedback formulae. The density of feedback points determines the computational accuracy in the domain, but the error does not increase much when the density is reduced from 1. Though a locally concentrated arrangement of feedback points in the targeted region intensively improve the computational accuracy, it is also affected by the error surrounding the region. Therefore, it is probably better to arrange somewhat large feedback domain with which the whole blood vessel is covered including the targeted region. The overall computational time needed to obtain periodic oscillation is substantially reduced by increasing the density of the feedback points by reduction of the transient state even with increased computational time in a fixed time step.

The effect of feedback outside the feedback domain was investigated by evaluating the error norm of each cross-section. Except for the case using the feedback domain located near the downstream boundary, the error in the velocity field decreases starting just before the feedback domain, continuing through it and persisting in some distance in the downstream region. Concerning the pressure field, feedback to the pressure equation moderates the error caused by the feedback to the momentum equations. This moderation in pressure field leads to convergence to the standard solution even in the UMI simulation using the feedback domain located near the upstream boundary.

As a fundamental consideration of optimization of feedback gains of feedback B, UMI simulation was performed for a two-dimensional parameter space of feedback gains for the momentum and pressure. Optimum gains were obtained for different error norms for the velocity, pressure, and their sum. It was confirmed that the limited condition using same values for two feedback gains for simplicity provides an approximate optimum result for the velocity, and the exact optimum for pressure and the sum of the two, justifying the limiting condition.

Acknowledgements

The present study was supported in part by research fellowship #16-3421 from the Japan Society for the Promotion of Science for Young Scientists. The authors wish to thank the Advanced Fluid Information Research Center, Institute of Fluid Science, Tohoku University, for support concerning computation.

References

(1) Caro, C.G., Fitz-Gerald, J.M. and Schroter, R.C., Atheroma and Arterial Wall Shear. Observation, Correlation and Proposal of a Shear-Dependent Mass Transfer Mechanism for Atherogenesis, Proc. R. Soc. Lond. B Biol. Sci., Vol.177, No.46 (1971), pp.109–159.

(2) Ku, D.N., Giddens, D.P., Zarins, C.K. and Glagov, S., Pulsatile Flow and Atherosclerosis in the Human Carotid Bifurcation. Positive Correlation between Plaque Location and Low Oscillating Shear Stress, Arteriosclerosis, Vol.5, No.3 (1985), pp.293–302.

(3) Giddens, D.P., Zarins, C.K. and Glagov, S., The Role of Fluid Mechanics in the Localization and Detection of Atherosclerosis, J. Biomech. Eng., Vol.115, No.4B (1993), pp.588–594.

(4) Flora, H.S., Talei-Faz, B., Ansdell, L., Chaloner, E.J., Sweeny, A., Grass, A. and Adiseshiah, M., Aneurysm Wall Stress and Tendency to Rupture Are Features of Physical Wall Properties: An Experimental Study, J. Endovasc. Ther., Vol.9, No.5 (2002), pp.665–675.

(5) DePaola, N., Gimbrone, M.A., Jr., Davies, P.F. and Dewey, C.F., Jr., Vascular Endothelium Responds to Fluid Shear Stress Gradients, Arterioscler. Thromb., Vol.12, No.11 (1992), pp.1254–1257.

(6) Davies, P.F., Mundel, T. and Barbee, K.A., A Mechanism for Heterogeneous Endothelial Responses to Flow In Vivo and In Vitro, J. Biomech., Vol.28, No.12 (1995), pp.1553–1560.

(7) Li, Z. and Kleinstreuer, C., A New Wall Shear Stress Equation for Aneurysm-Rupture Prediction, Ann. Biomed. Eng., Vol.33, No.2 (2005), pp.209–213.

(8) Ujiie, H., Tamano, Y., Sasaki, K. and Hori, T., Is the Aspect Ratio a Reliable Index for Predicting the Rupture of a Saccular Aneurysm?, Neurosurgery, Vol.48, No.3 (2001), pp.495–502.

(9) Steinman, D.A., Image-Based Computational Fluid Dynamics Modeling in Realistic Arterial Geometries, Ann. Biomed. Eng., Vol.30, No.4 (2002), pp.483–497.

(10) Di Martino, E.S., Guadagni, G., Fumero, A., Ballerini, G., Spirito, R., Biglioli, P. and Redaelli, A., Fluid-Structure Interaction within Realistic Three-Dimensional Models of the Aneurysmatic Aorta as a Guidance to Assess the Risk of Rupture of the Aneurysm, Med. Eng. Phys., Vol.23, No.9 (2001), pp.647–655.

(11) Liu, Y., Lai, Y., Nagaraj, A., Kane, B., Hamilton, A., Greene, R., McPherson, D.D. and Chandran, K.B., Pulsatile Flow Simulation in Arterial Vascular Seg-

ments with Intravascular Ultrasound Images, Med. Eng. Phys., Vol.23, No.8 (2001), pp.583–595.

(12) Glor, F.P., Westenberg, J.J., Vierendeels, J., Danilouchkine, M. and Verdonck, P., Validation of the Coupling of Magnetic Resonance Imaging Velocity Measurements with Computational Fluid Dynamics in a U Bend, Artif. Organs, Vol.26, No.7 (2002), pp.622–635.

(13) Marshall, I., Zhao, S., Papathanasopoulou, P., Hoskins, P. and Xu, X.Y., MRI and CFD Studies of Pulsatile Flow in Healthy and Stenosed Carotid Bifurcation Models, J. Biomech., Vol.37, No.5 (2004), pp.679–687.

(14) Papathanasopoulou, P., Zhao, S., Köhler, U., Robertson, M.B., Long, Q., Hoskins, P., Xu, X.Y. and Marshall, I., MRI Measurement of Time-Resolved Wall Shear Stress Vectors in a Carotid Bifurcation Model, and Comparison with CFD Predictions, J. Magn. Reson. Imaging, Vol.17, No.2 (2003), pp.153–162.

(15) Funamoto, K., Hayase, T., Shirai, A., Saijo, Y. and Yambe, T., Fundamental Study of Ultrasonic-Measurement-Integrated Simulation of Real Blood Flow in the Aorta, Ann. Biomed. Eng., Vol.33, No.4 (2005), pp.415–428.

(16) Hayase, T. and Hayashi, S., State Estimator of Flow as an Integrated Computational Method with the Feedback of Online Experimental Measurement, J. Fluids Eng., Vol.119, No.4 (1997), pp.814–822.

(17) Nisugi, K., Hayase, T. and Shirai, A., Fundamental Study of Hybrid Wind Tunnel Integrating Numerical Simulation and Experiment in Analysis of Flow Field, JSME Int. J., Ser.B, Vol.47, No.3 (2004), pp.593–604.

(18) Hayase, T., Nisugi, K. and Shirai, A., Numerical Realization for Analysis of Real Flows by Integrating Computation and Measurement, Int. J. Numer. Meth. Fluids, Vol.47 (2005), pp.543–559.

(19) Ferrara, K. and DeAngelis, G., Color Flow Mapping, Ultrasound Med. Biol., Vol.23, No.3 (1997), pp.321–345.

(20) Sakas, G., Trends in Medical Imaging: from 2D to 3D, Comput. Graph., Vol.26, No.4 (2002), pp.577–587.

(21) Capineri, L., Scabia, M. and Masotti, L., A Doppler System for Dynamic Vector Velocity Maps, Ultrasound Med. Biol., Vol.28, No.2 (2002), pp.237–248.

(22) Ohtsuki, S. and Tanaka, M., Doppler Pressure Field Deduced from the Doppler Velocity Field in an Observation Plane in a Fluid, Ultrasound Med. Biol., Vol.29, No.10 (2003), pp.1431–1438.

(23) Hayase, T., Humphrey, J.A.C. and Greif, R., Mini-Manual for ROTFLO2, Dept. Mech. Eng. Rep. FM-90-1, Univ. Calif., Berkeley, (1990).

(24) Patankar, S.V., Numerical Heat Transfer and Fluid Flow, (1980), Hemisphere Pub. Corp., Washington, D.C./New York.

(25) Ganong, W.F., Review of Medical Physiology, 17th Ed., (1995), p.555, Appleton & Lange, Norwalk, CT.

(26) Olufsen, M.S., Peskin, C.S., Kim, W.Y., Pedersen, E.M., Nadim, A. and Larsen, J., Numerical Simulation and Experimental Validation of Blood Flow in Arteries with Structured-Tree Outflow Conditions, Ann. Biomed. Eng., Vol.28, No.11 (2000), pp.1281–1299.